LA-UR -91-2834

LA-UR--91-2834

DE92 000317

Los Alamos National Laboratory is operated by the University of California for the United States Department of Energy under contract W-7405-ENG-36

TITLE: High-Voltage Virtual-Cathode Microwave Simulations

AUTHOR(S): Lester Thode
Charles M. Snell

SUBMITTED TO: Italian Physical society (Il Nuovo Cimento)
Varenna, Italy

DISCLAIMER

Los Alamos National Laboratory
Los Alamos, New Mexico 87545

FORM NO. 836 R4
ST. NO. 2629 5/81

High-Voltage Virtual-Cathode Microwave Simulations

L. E. Thode and C. M. Snell
Los Alamos National Laboratory
Los Alamos, NM 87545

Abstract

In contrast to a conventional microwave tube, a virtual-cathode device operates above the space-charge limit where the depth of the space-charge potential is sufficiently large to cause electron reflection. The region associated with electron reflection is referred to as a virtual cathode. Microwaves can be generated through oscillations in the position of the virtual cathode and by reflexing electrons trapped in the potential well formed between the real and virtual cathodes. A virtual-cathode device based on the first mechanism is a vircator while one based on latter mechanism is a reflex diode. A large number of low-voltage virtual-cathode microwave configurations have been investigated. Initial simulations of a high-voltage virtual-cathode device using a self-consistent particle-in-cell code indicated reasonable conversion efficiency with no frequency chirping. The nonchirping character of the high-voltage virtual-cathode device lead to the interesting possibility of locking four very-high-power microwave devices together using the four transmission lines available at Aurora. Subsequently, in support of two high-voltage experiments, simulations were used to investigate the effect of field-emission threshold and velvet position on the cathode; anode and cathode shape; anode-cathode gap spacing; output waveguide radius; diode voltage; a cathode-coaxial-cavity resonator; a high-frequency ac-voltage drive; anode foil scattering and energy loss; and ion emission on the microwave frequency and power. Microwave generation efficiency is sensitive to the nonideal effects of anode foil scattering, energy loss, and ion emission. As a result, the efficiency of a high-voltage virtual-cathode device is low.

I. INTRODUCTION

Aurora is the largest high-voltage, high-impedance electron beam generator in existence. The high-voltage generator can power four separate diodes through four separate 50-ohm coaxial transmission lines. With a typical transmission line voltage of 6-to-9 MV, the current in each transmission line is 120-to-180 kA. Thus, a peak power of 0.7-to-1.6 TW can be delivered to a matched diode. The FWHM voltage pulse width is about 135 ns.

With a diode voltage of 6-to-9 MV, a virtual-cathode microwave experiment on Aurora represents a major scaling for this class of high-power microwave device. Based upon previous research, a reasonable expectation for the efficiency of a well-designed virtual-cathode device is about 3%. Given that efficiency, a virtual-cathode device could generate a maximum average power of 20-to-48 GW and a total energy content of 2.7-to-6.5 kJ. In addition, unlike a virtual-cathode device energized with a low-voltage generator, initial particle-in-cell simulations indicated little frequency chirping when a virtual-cathode device is energized with a high-voltage generator. This high-voltage characteristic of the virtual-cathode device lead to the interesting possibility of locking four very-high-power microwave devices together using the four transmission lines available at Aurora.

The initial Aurora experiment used only one of the four transmission lines. [1] Basically, the main emphasis of this experiment was to establish that significant microwave power could be generated without diode collapse. Both axial and transverse extraction of the microwave power was possible. In this context, axial extraction refers to a configuration where the microwave power is extracted through an output waveguide with its axis aligned with the cathode axis. In the case of transverse extraction, the axial output waveguide is truncated to form a cavity and microwave power is extracted from the cavity in the transverse direction, perpendicular to the cathode axis, through rectangular waveguide. In the initial Aurora experiment two transverse waveguides were used in the transverse-extraction configuration. Subsequently, two additional experiments have been conducted in which the number of transverse waveguides has been increased. [2,3]

A similar virtual-cathode device was investigated experimentally using the PR1590, a 5-to-7 MV generator with a single diode driven by a 30-ohm coaxial transmission line. These microwave experiments were approximately a one-half and one-third scale version of the Aurora experiment. [4,5] However, the PR1590 experiment utilized only a single rectangular waveguide in the transverse configuration. Unlike the Aurora experiment, the microwave power was radiated in the PR1590 axial configuration.

CCUBE and ISIS were used to investigate the Aurora and PR1590 experiments. Both CCUBE and ISIS are two-dimensional, electromagnetic, relativistic particle-in-cell plasma simulation codes. For these codes the solution to a virtual-cathode device is obtained in dimensionless variables. Since the PR1590 experiments were scaled from the Aurora design a given simulation is applicable to both experimental configurations. The main difference between the Aurora and PR1590 experiments is the slightly lower voltage associated with the PR1590.

In Sec. II some aspects of the simulation design are discussed, including spatial zoning, time step, and microwave diagnostics. Five different virtual-cathode microwave configurations have been investigated. The motivation for considering each configuration is discussed in Sec. III. The effect of the field-emission threshold and velvet position on diode voltage and impedance as well as microwave power and energy is discussed in Sec. IV. In the Aurora experiment, it was necessary to modify the anode and cathode shape to achieve consistent high-power operation. The effect of these minor modifications to the anode and cathode shape is investigated in Sec. V. To investigate the virtual-cathode device sensitivity, the effect of anode-cathode gap spacing, output waveguide radius, and diode voltage on frequency and power was investigated. This information is summarized in Secs. VI through VIII, respectively. The effect of a cathode-coaxial-cavity resonator and ac-voltage drive on the microwave frequency and power is discussed in Secs. IX and X. Finally, the nonideal

effects of anode foil scattering, energy loss, and ion emission on microwave generation is discussed in Secs. XI and XII. A brief conclusion is given in Sec. XIII.

II. SIMULATION DESIGN AND DIAGNOSTICS

To obtain an accurate calculation of a virtual-cathode device using a particle-in-cell plasma simulation code, it is necessary to adequately resolve the axial wavelength, the transverse mode, and the frequency associated with the microwave output. In addition, there are basic constraints on the mesh size and time step associated with the electron density in the virtual-cathode region and the solution of Maxwell's Equations. In the case of CCUBE and ISIS the current is averaged in space to reduce high-frequency numerical noise, averaging which must be taken into account when the mesh size is determined.

Typically, ten mesh points per wavelength provides adequate resolution in space. For the Aurora and PR1590 simulations the coordinate system is cylindrical and azimuthally symmetric with a mesh size of $\Delta z/\lambda_E = \Delta r/\lambda_E = 1$, where λ_E is the electromagnetic skin depth. This spatial zoning is sufficient to resolve modes up to TM_{06}. The maximum time step is then determined by the Courant condition, which depends upon the mesh size and metric associated with a particular geometry. Essentially, this time-step limit implies that an electron cannot pass through the smallest cell in the mesh in single time step. Generally, such a time step provides adequate time resolution for the a virtual-cathode device. However, in some configurations it is necessary to use a smaller time step to resolve the plasma frequency in the virtual-cathode region.

With adequate resolution it is expensive to simulate the entire experimental time scale, especially when an experiment operates above C-band. However, because of the large dimensions associated with the Aurora experiment the frequency is in L-band. Thus, the entire 160-ns experiment can be simulated in about six hours on a CRAY computer.

In the Aurora simulations a TEM wave is launched onto the 50-ohm coaxial transmission line and the self-consistent voltage pulse resulting from mismatches between the transmission line and diode is calculated, including the magnetic insulation. The standard applied voltage is modeled as a trapezoidal pulse with a 70-ns risetime, a 20-ns flattop, and a 70-ns falltime, with a peak voltage of 10.7 MV. This voltage pulse shape is a reasonable approximation to the actual Aurora pulse. The actual diode voltage depends upon the magnetic insulation and diode impedance.

The microwave output associated with the virtual-cathode device can be very complex. On the whole, the frequencies can be time-dependent and the power is often distributed amongst a number of modes causing spiky or modulated output. Consequently, standard simulation diagnostics are wholly inadequate for virtual-cathode device calculations. To gain

useful information it is necessary to use extensive postprocessing capability coupled with a number of specialized diagnostics.

Both the electric and magnetic fields are expanded in terms of Bessel functions associated with TM_{0n} waveguide eigenmodes. In this fashion, the mode amplitudes, or coefficients, are determined. Given these time-dependent coefficients the frequency, wavelength, and power associated with a mode can be determined. For each mode, filtering can be used to remove contributions below cutoff, if desired. Recall that the number of modes depends upon the spatial zoning.

As stated previously, the instantaneous microwave power is often spiky and modulated. As such, a clear mode pattern begins to emerge only after time averaging. Average microwave power is calculated by three separate techniques. First, the radial electric field, E_r, and azimuthal magnetic field, B_θ, for a particular mode are used to calculate individual mode power. At the same time, the mode power can be determined using the axial electric field, E_z, once the frequency is known. With either approach, the total power is then obtained by summing up the separate mode contributions. Finally, the total poynting flux can be filtered and integrated across an output waveguide cross section. In test simulations with a single frequency, constant amplitude wave the separate techniques yield results within about five percent of one another. But with the chaotic character exhibited by a virtual-cathode device the agreement between the techniques is far worse, 20 to 30%, provided the electron beam space-charge contribution is properly removed. Basically, as is true experimentally, it is very difficult to obtain an accurate power measurement for a virtual-cathode device. In the tables, the stated microwave power and energy are obtained from the filtered poynting vector integrated across the output waveguide cross section.

Additional diagnostics are used to obtain the time-dependent beam current-density components at the anode. With filtering both the ac- and dc-current components are obtained. As with the fields, the axial and radial beam current densities are expanded into a Bessel series. In addition, the time-dependent diode voltage and impedance, beam current, and residual beam current down the output waveguide are monitored. Of course, the standard particle phase space and field information is available.

To determine the energy exchange between the electron beam and microwaves, radial mode integrals of $j_z E_z$ and $j_r E_r$ are monitored in the diode region, virtual-cathode region, and at specified positions along the output waveguide. These diagnostics show that energy is removed from the electron beam in the region between the cathode and the virtual cathode. Both the axial and radial current density components contribute to the microwave generation.

III. VIRTUAL-CATHODE MICROWAVE DEVICE CONFIGURATIONS

Five different diode configurations have been investigated, although the major dimensions of the coaxial transmission line, anode, and cathode remained fixed. In addition, the output waveguide radius remained fixed, except for the case summarized in Sec. VII, Table IV.

There was concern that a virtual cathode could not form at high voltage with the large anode-cathode gap needed to avoid diode collapse. Based upon previous experimental experience with a radiography diode, a 25-cm anode-cathode gap was required to avoid diode closure. Thus, most of the simulations have been performed with this standard anode-cathode gap spacing, except for the cases summarized in Sec. VI, Table III. From the simulations, in the 6-to-10 MV regime a virtual-cathode can always form, but the formation time depends upon the field-emission threshold.

The first configuration investigated is depicted in Fig. 1. A 50-ohm coaxial transmission line is used to feed a right-circular-cylinder diode with a 45-degree bevel at the tip. In all cases the cathode radius is 26.5 cm and the bevel starts 2.5 cm from the cathode face. A grounded transparent anode foil separates the diode from the 60.5-cm-radius output waveguide. The boundary condition on the output waveguide, which is located 250 cm from the anode foil, transmits microwaves with phase velocities near the speed of light.

Fig. 1. Simulation configuration #1 for the initial reflex diode geometry fielded on the Aurora experiment. In the simulation the 45-degree bevel is approximated with a stair-step pattern. The diagram scale is depicted in the lower right corner of the figure.

Cathode shank emission and subsequent magnetic insulation are important in virtual-cathode device operation. The standard simulation assumes a field-emission threshold of 200 keV/cm on the cathode shank, 45-degree bevel, and cathode face. In the experiment the cathode shank and 45-degree bevel were ultimately covered with velvet to reduce the field-emission threshold, as an option to increase the microwave output. In fact, with velvet on the cathode the microwave output was observed to increase significantly in the experiment. Unfortunately, the thickness of the anode screen was reduced at the same time. Thus, it was not clear if the presence of the velvet or the reduction in anode screen thickness was responsible for the increased microwave power. As a result, simulations performed subsequent to the experiment investigated the impact of the field-emission threshold and velvet position on microwave generation. Configuration #1 was used for this investigation.

The anode screen was not changed for each experiment. Typically, about four experiments could be conducted before the anode screen needed to be replaced. In each series of experiments the anode screen was initially uniform, as indicated in Fig. 1, but a 7.5-cm radius axisymmetric hole was formed in the anode after the diode was energized. The configuration shown in Fig. 2 was used to investigate the effect of this anode screen modification on microwave generation. Except for the axisymmetric hole in the anode screen, configuration #2 is identical to configuration #1.

Fig. 2. Simulation configuration #2 for the initial reflex diode geometry with a 7.5-cm radius hole in the anode screen. Energy deposited by reflexing electrons appears to be the source of the anode hole.

During the initial experiment the front face of the aluminum cathode had to be modified. Large amounts aluminum were vaporized from the front face of the cathode during the late time voltage reversal of the Aurora pulse. To solve this problem, a cathode with a 7.5-cm radius hole in the front face replaced the original cathode. Since the inside of the cathode was hollow, the hole in the cathode face opened up into a large cavity with a rather ill-defined rear boundary, due to the presence of struts. A reasonable approximation to the modified cathode is shown Fig. 3. Except for the modification to the cathode, configuration #3 is identical to configuration #2.

There was an indication that the microwave power was larger with a hole present in the anode screen. Thus, despite the high voltage, it was suspected that scattering and energy loss in the anode screen might be important. To investigate the effect of anode foil scattering and energy loss on the microwave power the configuration shown in Fig. 4 was used. In this case the anode foil was allowed to scatter and remove energy from the electrons as they repeatedly passed through the anode. Except for the anode foil, configuration #4 is identical to configuration #3.

Fig. 3. Simulation configuration #3 for the final reflex diode geometry fielded in the Aurora experiment. A 7.5-cm hole is present in both the anode screen and cathode face. In the experiment the end boundary of the internal cavity, opposite the hole in the cathode face, was three-dimensional due to the presence of struts. Since CCUBE is only two-dimensional in space it was necessary to approximate the end boundary as shown.

The simulations show the presence of a coherent reflexing component of current centered about the anode-cathode axis. In an attempt to control this reflexing current, a number of simulations were carried out with a cathode-coaxial-cavity resonator, configuration #5, as opposed to the large open cavity present in configurations #2 and #4. Conceptually, the three-quarter wavelength coaxial cavity dimensions were selected to resonate with the reflexing current. The cathode-coaxial-cavity resonator configuration is depicted in Fig. 5. Except for the cathode, configuration #5 is identical to configuration #3.

Fig. 4. Simulation configuration #4 for final reflex diode geometry fielded in the Aurora experiment but with no hole in the anode.

IV. FIELD-EMISSION THRESHOLD AND VELVET POSITION

The initial cathode was made of aluminum. However, during the experiment velvet was placed on the cathode shank and the 45-degree bevel in an attempt to improve the microwave generation efficiency. At the same time, the thickness of the anode screen was significantly reduced. These two modifications lead to an increase in microwave power. Unfortunately, it was not possible to determine if the increased microwave power was due to improved cathode emission or reduced anode screen scattering and energy loss. Thus, a number of simulations were performed to investigate the effect of the field-emission threshold on the microwave efficiency. In the simulations the regions of the cathode covered with velvet are modeled by reducing the field-emission threshold to 20 keV/cm.

Fig. 5. Simulation configuration #5 for a reflex diode with a cathode-coaxial-cavity resonator.

The field-emission threshold simulations are summarized in Table I. For reference, a simulation designator is given in column 1. The simulation configuration used for a particular simulation is indicated in column 2. For the field-emission threshold and velvet position investigation only configuration #1 was considered. In columns 3 and 4 are the field-emission thresholds assumed for aluminum and velvet, respectively. If present, the velvet position is indicated in column 5. In this instance, shank refers to the cathode edge, or shank, while bevel refers to the 45-degree bevel. All the simulations have a noninteracting anode foil - no anode scattering or energy loss. Over the stated time interval, the time averaged diode voltage, diode impedance, and microwave power are given in columns 6 through 8. Finally, the microwave energy generated during the time interval is provided in column 9.

The highest microwave energy and power is achieved with a metal cathode at a field-emission threshold of 500 keV/cm. This is an indication that the slope of the bevel might be important, provided such a high field-emission threshold were possible. The position of the velvet on the cathode can affect the microwave power and energy, compare simulations AC and AG in Table I.

Note that the average diode impedance over the entire pulse increases as the field-emission threshold increases, because the diode cannot emit electrons until much later in the

voltage pulse. In contrast, the diode impedance during the peak of the voltage pulse is about the same for the five cases considered.

In summary, based on the field-emission threshold and velvet position simulations, velvet is not responsible for the increased microwave power in the experiment. On the other hand, as a point to consider in the future, the fraction of the power in the TM_{01} mode and, to a lesser extent, the frequency does depend upon the cathode field-emission threshold.

Run	#	E(keV/cm) metal	E(keV/cm) velvet	velvet position	V(MV)	Z(ohm)	P(GW)	E(kJ)
AA	(1)	200	none	none	4.90	43.1	30.1	4.83
AB	(1)	300	none	none	5.00	53.7	30.0	4.84
AF	(1)	500	none	none	5.09	82.5	38.9	6.22
AC	(1)	300	20	shank, bevel	4.82	35.4	30.1	4.82
AG	(1)	300	20	bevel	4.75	34.4	32.5	5.20
AA	(1)	200	none	none	8.40	33.1	67.5	1.35
AB	(1)	300	none	none	8.60	34.2	69.0	1.38
AF	(1)	500	none	none	8.60	34.9	77.5	1.55
AC	(1)	300	20	shank, bevel	8.25	32.2	69.0	1.38
AG	(1)	300	20	bevel	8.00	30.5	63.0	1.26

Table I. Simulation results for field-emission threshold and velvet position on the cathode. The first five rows are data averaged from 0 to 160 ns while the last five rows are data averaged from 78 to 98 ns, which corresponds to the 20-ns flattop of the voltage pulse.

V. ANODE AND CATHODE SHAPE

A summary of the effect of minor modifications in the anode and cathode shape is given in Table II. Recall that configuration #1 corresponds to the initial Aurora experimental geometry while configuration #3 is the final Aurora experimental geometry. The intermediate geometry, configuration #2, was considered to isolate the effect of the anode hole. In all cases, velvet was present on the cathode shank and 45-degree bevel at a 20 keV/cm field-emission threshold. The aluminum field-emission threshold is 300 keV/cm, see simulation AC in Table I. All the simulations have a noninteracting anode foil. Columns 3 and 4 indicate the shape of the cathode and anode geometry. The fraction of the microwave energy contained in TM_{01} mode is given in column 5. Over the stated time interval, the time averaged diode voltage, diode impedance, and microwave power are given in columns 6 through 8. Finally, the microwave energy generated during the time interval is provided in column 9.

Comparing the three configurations, there is little difference in the diode impedance, microwave power, or microwave energy. The microwave pulse length and frequency associated with the three configurations are essentially the same. However, the fraction of

the power contained in the TM_{01} mode is slightly different. In summary, at least in the absence of anode foil scattering and energy loss, the minor modifications in the anode and cathode geometry are not significant with respect to the microwave power generated.

Run	#	anode	cathode	TM_{01}(%)	V(MV)	Z(ohm)	P(GW)	E(kJ)
AC	1	solid	solid	74	4.82	35.4	30.1	4.82
AD	2	hole	solid	81	4.83	34.8	27.9	4.47
AE	3	hole	hole	84	4.93	34.5	29.9	4.78
AC	1	solid	solid	74	8.25	32.2	69.0	1.38
AD	2	hole	solid	81	8.20	31.3	68.5	1.37
AE	3	hole	hole	84	8.45	32.7	71.5	1.43

Table II. Simulation results for minor modifications in cathode and anode shape. The first three rows are data averaged from 0 to 160 ns while the last three rows are data averaged from 78 to 98 ns, which corresponds to the 20-ns flattop of the voltage pulse.

VI. ANODE-CATHODE GAP SPACING

Simulation results for different anode-cathode gap spacings are summarized in Table III. In all cases, velvet was present on the cathode shank and 45-degree bevel. The aluminum field-emission threshold is 300 keV/cm, see simulation AC in Table I. All the simulations have a noninteracting anode foil. Column 3 gives the anode-cathode gap spacing.

The frequency data is presented in columns 4 and 5. For each anode-cathode gap spacing there are two frequency components: the lower component is attributed to reflexing electrons while the higher component is due to the oscillating virtual cathode. This relationship was determined by comparing the frequency spectrum for the standard anode foil with that of a finite thickness anode foil. In a standard simulation, the anode foil is defined by zeroing the radial electric field along a plane. For a one-cell-thick anode foil, the reflexing-electron frequency decreases while the oscillating-virtual-cathode frequency is basically unchanged. The frequency was determined from the Fourier transform of the axial electric field associated with TM_{01}. In all cases, the Fourier transform over the entire voltage pulse shows little chirping. This is in contrast to a low-voltage reflex diode where the effective bandwidth often approaches 50%.

Over the stated time interval, the time averaged diode voltage, diode impedance, and microwave power are given in columns 6 through 8. Finally, the microwave energy generated during the time interval is provided in column 9. From the data there is a trend of improved efficiency as the anode-cathode gap spacing is increased, at least from an anode-cathode gap of 20 cm to 25 cm.

In Fig. 6 the microwave frequency is plotted as a function of anode-cathode gap spacing. The frequency measured in the Aurora experiment is consistent with the simulation

prediction. In the PR1590 experiment the frequency increases as the anode-cathode gap spacing is decreased, as expected. Recall that the PR1590 experiments are a one-half and one-third scale design of the Aurora experiment. Thus, this experiment would exhibit a frequency twice and three times that of the Aurora experiment when energized by the same voltage pulse. The PR1590 data is scaled in this manner. Overall, the PR1590 data is consistent with the simulation results even though the experiment had a slightly lower diode voltage. Note that the predicted lower frequency component is observed in both of the PR1590 experiments.

Run	#	d(cm)	f(MHz) lower	f(MHz) upper	V(MV)	Z(ohm)	P(GW)	E(kJ)
AQ	3	20	335	785	4.61	32.6	28.6	4.57
AE	3	25	360	690	4.93	34.5	29.9	4.78
AR	3	30	315	560	5.03	36.2	31.5	5.04
AQ	3	20	385	805	7.80	28.4	54.0	1.08
AE	3	25	380	700	8.45	32.7	71.5	1.43
AR	3	30	310	585	8.90	36.6	70.0	1.40

Table III. Simulation results for anode-cathode gap variation. The first three rows are data averaged from 0 to 160 ns while the last three rows are data averaged from 78 to 98 ns, which corresponds to the 20-ns flattop of the voltage pulse.

Fig. 6. Microwave frequency as a function of anode-cathode gap spacing. The simulations and experiments are summarized in the legend.

VII. OUTPUT WAVEGUIDE RADIUS

Simulation results for two different output waveguide radii are summarized in Table IV. In both cases, velvet was present on the cathode shank and 45-degree bevel. The aluminum field-emission threshold is 300 keV/cm. All the simulations have a noninteracting anode foil. Columns 3 through 5 gives the output waveguide radius, the lower frequency, and the upper frequency, respectively. Over the stated time interval, the time averaged diode voltage, diode impedance, and microwave power are given in columns 6 through 8. Finally, the microwave energy generated during the time interval is provided in column 9.

The microwave power decreased significantly as the waveguide radius decreased. The reduction in microwave efficiency with radius results from weaker virtual-cathode formation.

Run	#	R(cm)	f (MHz) lower	f (MHz) upper	V(MV)	Z(ohm)	P(GW)	E(kJ)
AV	3	45	420	700	4.80	33.0	20.8	3.33
AE	3	60	360	690	4.93	34.5	29.9	4.78
AV	3	45	390	695	8.30	31.3	50.1	1.00
AE	3	60	380	700	8.45	32.7	71.5	1.43

Table IV. Summary of simulation results for anode-cathode gap variation. The first two rows are data averaged from 0 to 160 ns while the last two rows are data averaged from 78 to 98 ns, which corresponds to the 20-ns flattop of the voltage pulse.

VIII. DIODE VOLTAGE

The diode voltage depends upon the magnetic insulation and diode impedance. As an example, the applied voltage and diode voltage are shown as a function of time in Fig. 7. The simulation is AA, see Table I. In the figure, the trapezoidal voltage pulse indicated by the dashed line is the applied voltage to the transmission line. The actual diode voltage is indicated by the solid line. There is about a 3-ns delay in the diode voltage relative to the applied voltage because the measurements are made at slightly different positions. The applied voltage pulse is a right-going wave, whereas the diode voltage is the combination of the the right-going(incident) wave and left-going wave (reflected).

At about 15 ns into the pulse the 45-degree bevel begins to emit electrons. As the voltage continues to rise the cathode shank field-emission threshold is exceeded. Shank emission occurs at about 35 ns into the voltage pulse. As each region begins to emit electrons there is a change in the slope of the diode voltage, which is an indication of the mismatch between the coaxial-transmission-line impedance and the reflex-diode impedance.

A small amount of microwave power appears when the 45-degree bevel generates a low kinetic energy electron beam, but significant microwave power occurs only after the cathode shank contributes to the virtual cathode. Ninety percent of the microwave energy is generated within 80 ns, in the interval 55-to-135 ns.

Simulation results as a function of diode voltage are summarized in Table V. In all cases, velvet was present on the cathode shank and 45-degree bevel. The aluminum field-emission threshold is 300 keV/cm. All the simulations have a noninteracting anode foil. Columns 3 and 4 contain the lower and upper frequency associated with the TM_{01} mode. Over the stated time interval, the time averaged diode voltage, diode impedance, and microwave power are given in columns 5 through 7. Finally, the microwave energy generated during the time interval is provided in column 8.

The microwave power increases significantly as the voltage is increased. Since the diode impedance is weakly dependent upon the diode voltage, the microwave efficiency actually decreases slightly as the diode voltage increases. Thus, the significant increase in microwave power is really due to the increased beam power.

The frequency tends to increase as the diode voltage increases. Despite this trend toward higher frequency the microwave pulse exhibits little chirping. Basically, the bulk of the microwave energy is produced when the voltage remains near maximum, whereas the voltage variation simulations change the diode voltage significantly.

Fig. 7. Applied voltage and diode voltage as a function of time.

Run	#	f (MHz) lower	f (MHz) upper	V(MV)	Z(ohm)	P(GW)	E(kJ)
AT	3	320	540	2.48	35.3	5.93	0.95
AZ	3	340	570	3.71	35.1	14.3	2.29
AE	3	360	690	4.93	34.5	29.9	4.78
AU	3	380	780	7.25	33.9	66.8	10.7
AT	3	320	550	4.51	36.5	13.7	0.27
AZ	3	350	580	6.45	34.5	28.5	0.57
AE	3	380	700	8.45	32.7	71.5	1.43
AU	3	380	750	12.3	30.5	157.0	3.15

Table V. Summary of simulation results for diode voltage. The first four rows are data averaged from 0 to 160 ns while the last four rows are data averaged from 78 to 98 ns, which corresponds to the 20-ns flattop of the voltage pulse.

IX. CATHODE-COAXIAL-CAVITY RESONATOR

In Fig. 8 the axial current density at the anode foil is shown as a function of radius for simulation AA, see Table I. In the figure, r_{guide} is the radius of the output waveguide, which is 60.5 cm in the Aurora experiment. The solid line is the dc-current component of the current density while the dashed lines are the upper and lower extreme of the ac-current component. The data is averaged over the peak voltage interval of 78-to-98 ns. A negative current density corresponds to electrons entering the virtual-cathode region. In the figure, the vertical dashed line at $r = 0.44\ r_{guide}$ indicates the position of the cathode edge. Note that the incoming electron beam is annular with a modest return current flow back into the diode region near the axis. In contrast to the dc-current component, the ac-current component peaks on axis and is small at the cathode edge.

The vertical dashed line at $r = 0.12\ r_{guide}$ indicates the radius of the hole formed in the anode after the diode has been energized once, starting with an initially uniform anode foil. Each time the diode is energized the anode hole becomes slightly larger. From Fig.8, it is evident that the anode hole is located in the region where the reflexing-electron current is quite large. When energy loss is included in the simulation, it is possible to calculate the energy deposited in the anode foil as a function of radius. In fact, the energy deposition profile is similar to the reflexing current density profile. Thus, in the experiment, the anode hole appears to be caused by the intense reflexing-electron current located near the diode axis.

This large component of reflexing current density located near the diode axis suggests that a cathode-coaxial-cavity resonator might enhance the electron bunching in the reflex. The set of initial simulations investigating this idea is summarized in Table VI. The cathode-coaxial-cavity resonator length is stated in column 3. In the present set of simulations, the

length of the three-quarter wavelength cavity is chosen to be resonant with the reflexing current component. Because of the heavy beam loading, the cavity length was varied about this resonant condition. The last four columns in Table VI are the diode voltage, diode impedance, microwave power, and microwave energy.

Fig. 8. Axial current density as a function of radius at the anode foil.

Although there are changes in the frequency spectrum and fraction of power contained in TM_{01}, there is no indication of a significant increase in efficiency resulting from the presence of the cathode-coaxial-cavity resonator.

Run	#	length (cm)	f(MHz) lower	f(MHz) upper	V(MV)	Z(ohm)	P(GW)	E(kJ)
AS	5	26	330	680	4.98	35.9	30.4	4.87
AM	5	29	330	615	4.83	33.0	30.1	4.81
AI	5	32	300	640	4.87	33.9	28.0	4.48
AO	5	35	360	650	4.85	33.7	28.3	4.52
AS	5	26	-	-	8.40	32.5	70.0	1.40
AM	5	29	-	-	8.45	32.7	69.0	1.38
AI	5	32	-	-	8.35	32.1	72.0	1.44
AO	5	35	-	-	8.35	32.5	70.0	1.40

Table VI. Summary of coaxial-cavity cathode simulations. The first four rows are data averaged from 0 to 160 ns while the last four rows are data averaged from 78 to 98 ns, which corresponds to the 20-ns flattop of the voltage pulse.

X. HIGH-FREQUENCY AC-VOLTAGE DRIVE

A set of exploratory simulations was conducted to investigate the effect of an ac-voltage ripple on the microwave power. The results of these simulations are summarized in Table VII. In column 3 the ratio of the amplitude of the ac-voltage ripple to the instantaneous mean voltage is given. The ripple frequency was set equal to the reflexing-electron frequency in simulation AX. In contrast, the ripple frequency was set equal to the oscillating-virtual-cathode frequency in simulation AW. In each case, the ripple frequency is indicated in column 4. A slight enhancement in the driven frequency component was observed in both simulations, as indicated in column 5. The diode voltage, diode impedance, microwave power, and microwave energy are summarized in columns 6 through 9.

In short, these exploratory simulations indicated that a voltage ripple had slight impact on the microwave bunching process, but little overall impact on the total power was observed. On the other hand, there was an indication that the power spectrum was modified. No off-resonance voltage drive simulations were performed because the main interest was to improve the bunching efficiency. It is possible that an off-resonance ac ripple might be able to shift the frequency of the interaction, but no enhancement in overall efficiency should be expected.

Run	#	E_{ac}(%)	f (MHz) drive	f (MHz) enhanced	V(MV)	Z(ohm)	P(GW)	E(kJ)
AE	3	0	none	none	4.98	35.9	30.4	4.87
AX	3	10	360	360	4.83	33.0	30.1	4.81
AW	3	10	710	710	4.87	33.9	28.0	4.48
AE	3	0	none	none	8.40	32.5	70.0	1.40
AX	3	10	360	360	8.45	32.7	69.0	1.38
AW	3	10	710	710	8.35	32.1	72.0	1.44

Table VII. Summary of ac ripple voltage simulations. The first three rows are data averaged from 0 to 160 ns while the last three rows are data averaged from 78 to 98 ns, which corresponds to the 20-ns flattop of the voltage pulse.

XI. ANODE FOIL SCATTERING AND ENERGY LOSS

The initial anode on the Aurora experiment was a 1.27-mm, stainless-steel mesh screen with an optical transparency of about 60%. Defining the effective anode foil thickness as the actual wire thickness times the area of the wire divided by the total area of anode, this anode had an effective thickness of about 400 mg/cm2. With this geometry the microwave output was much lower than expected, compared with initial simulation predictions. Thus, as stated before, two modifications were made to the experiment: 1) velvet was placed on the cathode shank and 45-degree bevel and 2) the anode was changed to a 0.25-mm, aluminum mesh

screen. The anode screen transparency remained about 60%. This thinner anode had an effective thickness of about 30 mg/cm2. These two modifications in the geometry caused a significant increase in the microwave power.

Given the null impact of velvet on microwave power, as discussed in Sec. IV, the effect of anode foil scattering and energy loss on high-voltage reflex diode operation was investigated. It is well established that low-voltage reflex diodes are sensitive to anode foil thickness. However, one potential advantage of a high-voltage reflex diode was thought to be reduced sensitivity to anode foil scattering and energy loss.

The results of anode foil scattering and energy loss simulations are summarized in Table VIII. Configurations #3 and #4 were both considered to determine the effect of the hole in the anode with foil scattering and energy loss present. In the simulations the anode is modeled as a solid foil, not a screen. With some code modification it appears possible to approximate a partially transparent anode, but the technique has not been implemented.

The presence (yes) or absence (no) of a hole in the anode foil, anode scattering, and anode energy loss are indicated in columns 3 through 5, respectively. In column 6 the aluminum anode foil thickness is given. In terms of effective thickness, the thickest anode foil considered in the simulations is the thinnest anode screen used in the experiment. Finally, the last four columns in Table VIII are the diode voltage, diode impedance, microwave power, and microwave energy.

Compare simulations AL and AJ with an anode thickness of 6.86 mg/cm2 and simulations AK and AN with an anode thickness of 34.3 mg/cm2. In both instances, the anode scattering is responsible for bulk of the reduction of the microwave output, with an additional 10-to-15% reduction in microwave power resulting from energy loss. When anode foil scattering and energy loss are included, the high-frequency component is reduced more than the low-frequency component. This implies that the transverse extraction geometry is more sensitive to anode foil scattering and energy loss than the axial extraction geometry, since the low-frequency component is cutoff in the rectangular waveguide.

The anode hole slightly reduces the sensitivity of the reflex diode to anode foil scattering and energy loss. This can be seen by comparing simulations AP and AJ.

Based upon these simulation results, the reduction of the anode screen thickness in the experiment was responsible for the increased microwave power. Moreover, the expected reflex diode power is reduced about a factor of two by anode foil scattering. In fact, the high-voltage reflex diode is as sensitive to anode foil scattering and energy loss as the low voltage reflex diode.

Run	#	anode	θ	ΔE	δ(mg/cm2)	V(MV)	Z(ohm)	P(GW)	E(kJ)
AE	3	hole	no	no	0	4.93	34.5	29.9	4.78
AP	3	hole	yes	yes	6.86	5.11	35.9	22.9	3.66
AL	4	solid	yes	no	6.86	5.16	36.6	24.8	3.96
AJ	4	solid	yes	yes	6.86	5.10	37.0	21.6	3.46
AK	4	solid	yes	no	34.3	5.11	41.6	18.2	2.91
AN	4	solid	yes	yes	34.3	5.13	36.3	16.9	2.71
AE	3	hole	no	no	0	8.45	32.7	71.5	1.43
AP	3	hole	yes	yes	6.86	8.85	35.1	47.8	0.96
AL	4	solid	yes	no	6.86	8.80	34.7	42.3	0.85
AJ	4	solid	yes	yes	6.86	8.75	34.7	49.4	0.99
AK	4	solid	yes	no	34.3	8.65	33.8	40.7	0.81
AN	4	solid	yes	yes	34.3	8.75	34.6	36.1	0.72

Table VIII. Simulation results for anode scattering and energy loss. The first six rows are data averaged from 0 to 160 ns while the last six rows are data averaged from 78 to 98 ns, which corresponds to the 20-ns flattop of the voltage pulse.

XII. ION GENERATION

Energetic ions were measured in the Aurora experiment. This limited simulation investigation was only intended to gain understanding of the sensitivity of the diode impedance and microwave generation on ion emission.

A summary of the diode voltage, current, and impedance for each simulation is given in Table IX. Column 3 indicates which code, CCUBE or ISIS, was used. The voltage pulse length is indicated in column 4. For the 160-ns pulse the risetime is 70-ns, the flattop is 20-ns, and the falltime is 70-ns. For the 27-ns pulse the risetime is 7-ns and the flattop 20-ns. These shorter simulations investigated the effect of ever increasing ion emission from the anode. If ion emission is included in the simulation, it is indicated in column 5. Finally, the average voltage, current, and impedance associated with the 20-ns flattop are given in columns 6 through 8, respectively.

Run	#	code	pulse length (ns)	ions	V(MV)	I(kA)	Z(ohm)
AC	3	CCUBE	160	no	8.40	254	33.1
AE	3	CCUBE	160	no	8.45	258	32.7
IA	3	ISIS	160	no	8.15	263	31.0
IE	3	ISIS	160	yes	8.00	265	30.2
IC	3	ISIS	27	no	9.10	285	31.8
ID	3	ISIS	27	yes	9.05	285	31.7
IF	3	ISIS	27	yes	8.65	291	29.7
IG	3	ISIS	27	yes	8.30	299	27.7

Table IX. Diode voltage, current, and impedance obtained from CCUBE and ISIS.

In previous simulations of the Aurora reflex diode the code CCUBE was used. However, CCUBE does not have an ion emission algorithm. As a result, ISIS was used in the investigation of ion generation and acceleration.

As a starting point, simulation IA was a check against simulation AE. From Table IX, the difference between CCUBE and ISIS with respect to diode voltage, current, and impedance is about five percent, which is reasonable.

Ion emission was then allowed to occur in simulation IE, which is identical in all other respects to simulation IA. In particular, ions were allowed to emit in an annular region associated with the reflexing current. From Table IX the diode impedance was reduced very slightly with ion emission.

Because of the unexpected small change in the diode impedance observed in simulation IE, a series of test simulations were carried out to investigate the effect of changes as ion emission occurred over a larger region of the anode. As the ion emission increased, the reduction in diode voltage and impedance increased, see simulations IC, ID, IF and IG. Even with ion emission over the entire region of electron beam interaction with the anode, the voltage and impedance drop was only 15%.

Despite the modest change in diode voltage and impedance, the electron beam trajectories are highly modified when significant ion emission occurs. As the ion emission is increased the incoming electron beam radius is reduced. In other words, the electron beam begins to pinch with ions present near the diode axis. In addition, the average beam plasma frequency tends to increase because of the increased current density and decreased diode voltage. As a result, the microwave frequency tends to increase.

Finally, with a large number of ions present in the source region microwave generation appears to quench. For example, in simulation IG the microwave power was rapidly quenching after about 20 ns.

XIII. CONCLUSION

A large number of simulations have been performed to investigate high-voltage reflex diode operation.

None of the effects investigated lead to enhanced performance. On the negative side, the nonideal effects of anode foil scattering, anode foil energy loss, and anode ion emission can significantly reduce microwave power.

ACKNOWLEDGMENTS

The authors gratefully acknowledge G. Huttlin and M. Haworth for many informative discussions concerning the Aurora and PR1590 experiments. This research was supported by the U. S. Department of Energy and the Strategic Defense Initiative Office of Innovative Science and Technology.

REFERENCES

1. A. Bromborsky, F. Agee, M. Bollen, J. Cameron, C. Clark, H. Davis, W. Destler, S. Graybill, G. Huttlin, D. Judy, R. Kehs, R. Kribel, L. Libelo, J. Pasour, N. Pereira, J. Rodgers, M. Rubush, B. Ruth, C. Schlesiger, E. Sherwood, L. Smutek, G. Still, L. Thode, and D. Weidenheimer," On the Path to a Terawatt: High Power Microwave Experiments at Aurora," SPIE **873**, 51 (1988).

2. G. A. Huttlin, M. S. Bushell, D. P. Davis, D. C. Judy, M. S. Litz, N. R. Pereira, L. Smutek, D. M. Weidenheimer, F. J. Agee, W. M. Bollen, A. Bromborsky, C. Ford, K. Gentile, J. Pasour, C. D. R. Schlesiger, " Generating High-Power Microwaves with the Aurora Pulser, " SPIE **1061**, 24 (1989).

3. G. A. Huttlin, M. S. Bushell, D. B. Conrad, D. P. Davis, K. L. Ebersole, D. C. Judy, P. A. Lezcano, M. S. Litz, N. R. Pereira, B. G. Ruth, D. M. Weidenheimer, and F. J. Agee, " Reflex-Diode High-Power Microwave Source on Aurora, " SPIE **1226**, 147 (1990).

4. R. Platt, B. Anderson, J. Christofferson, J. Enns, M. Haworth, J. Metz, P. Pelletier, R. Rupp, and D. Voss, " Low-Frequency, Multigigawatt Microwave Pulses Generated by a Virtual Cathode Oscillator, " Appl. Phys. Lett. **54**, 1215 (1989).

5. M. Haworth, R. Adler, B. Anderson, M. Connaughton, W. Dungan, J. Enns, J. Metz, P. Pelletier, R. Platt, J. Polaco, R. Rupp, L. Thode, and D. Voss, " Experimental Observation of Two Microwave Radiation Mechanisms with Widely Separated Frequencies During the Output Pulse of a High-Voltage Virtual Cathode Oscillator, Appl. Phys. Lett. **59**, 408 (1991).

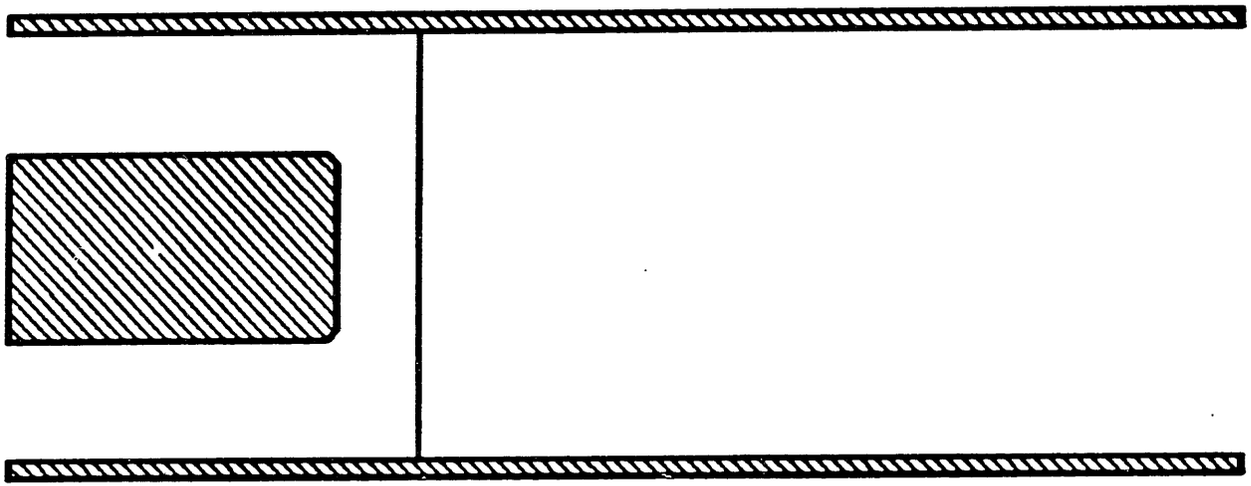

Fig. 1

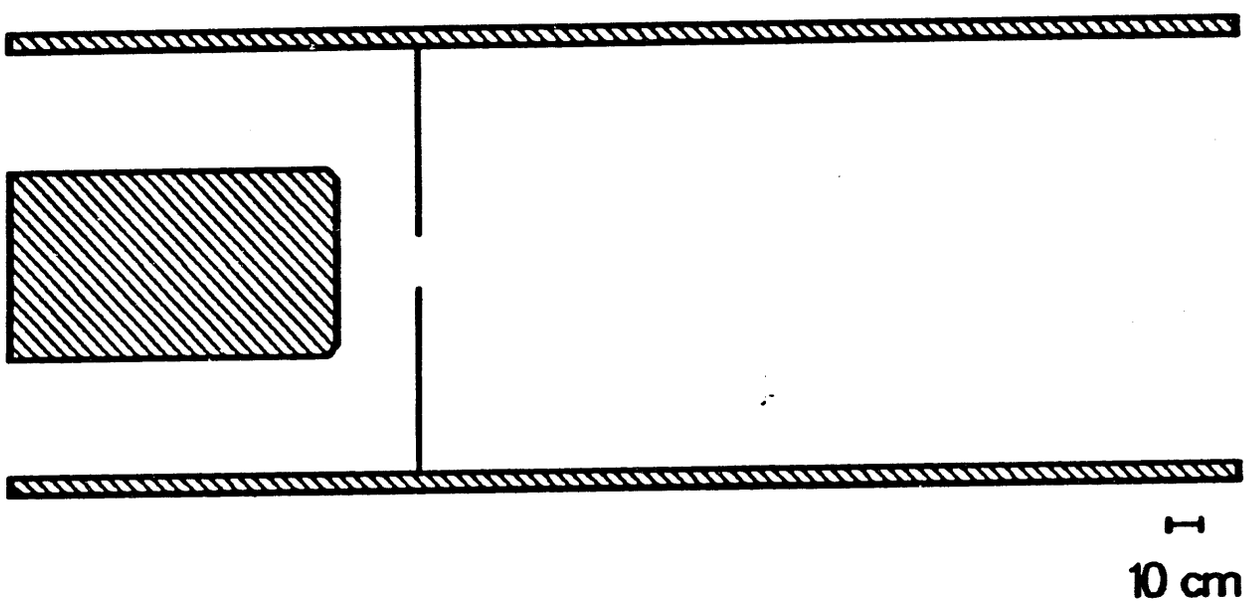

Fig. 2.

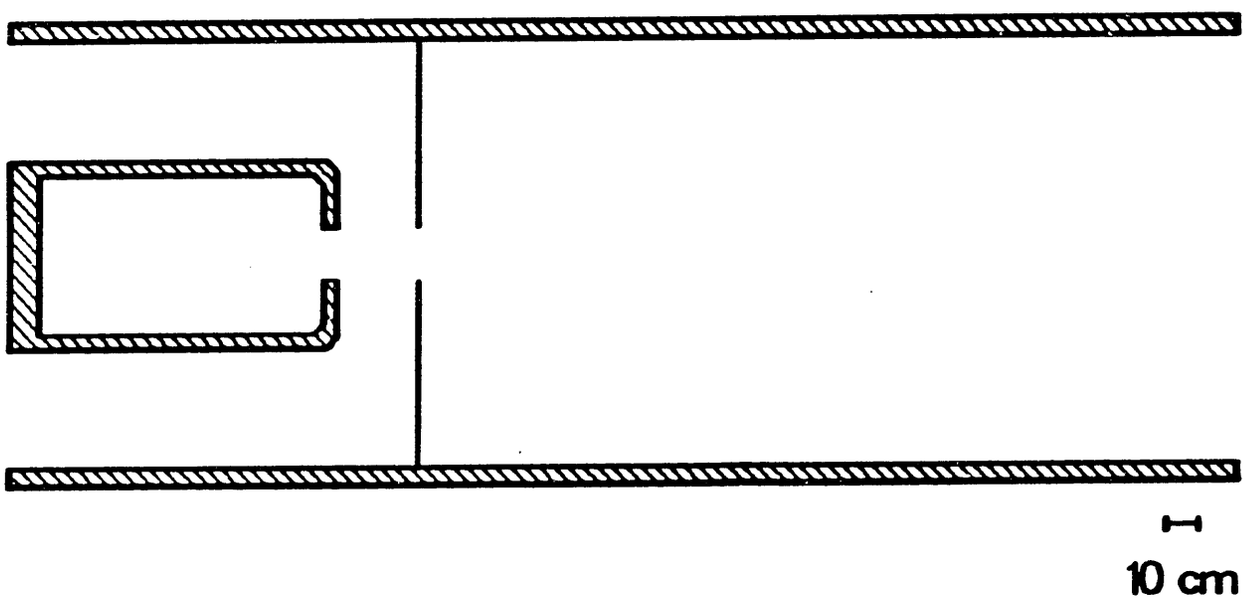

Fig. 3.

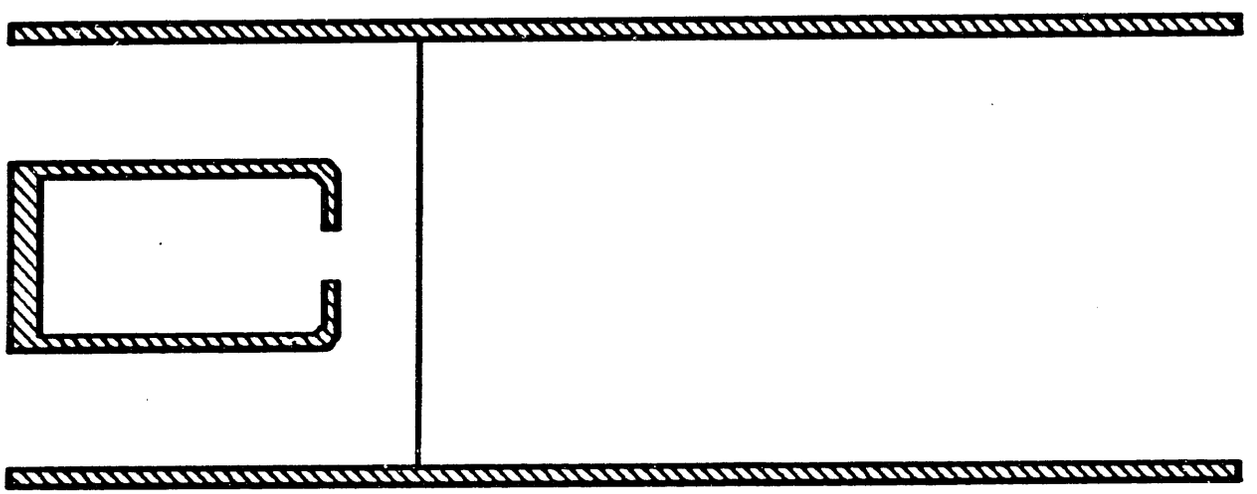

Fig. 4

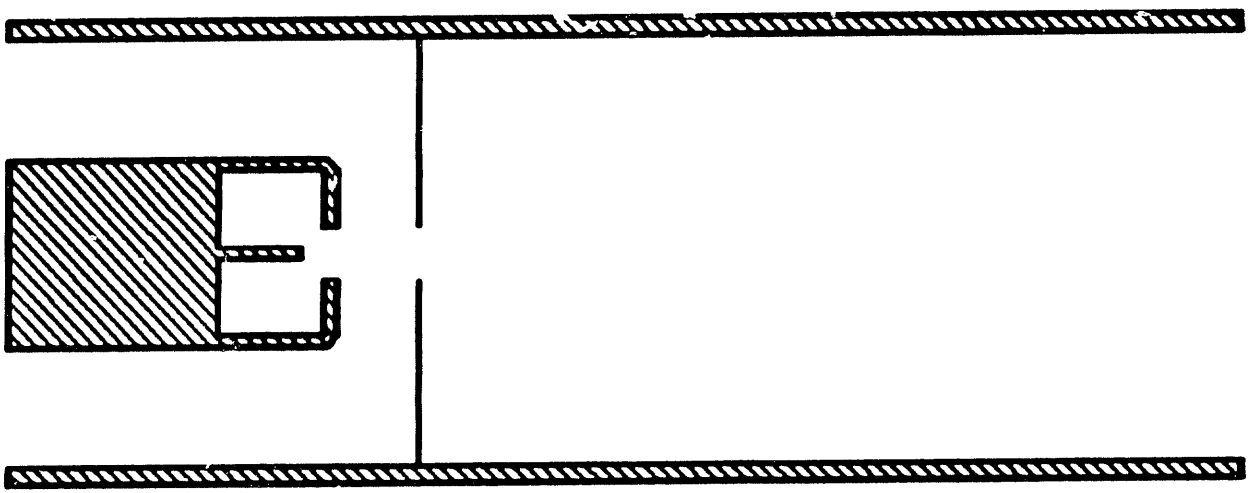

Fig 5

FREQUENCY DECREASES WITH ANODE-CATHODE GAP SPACING

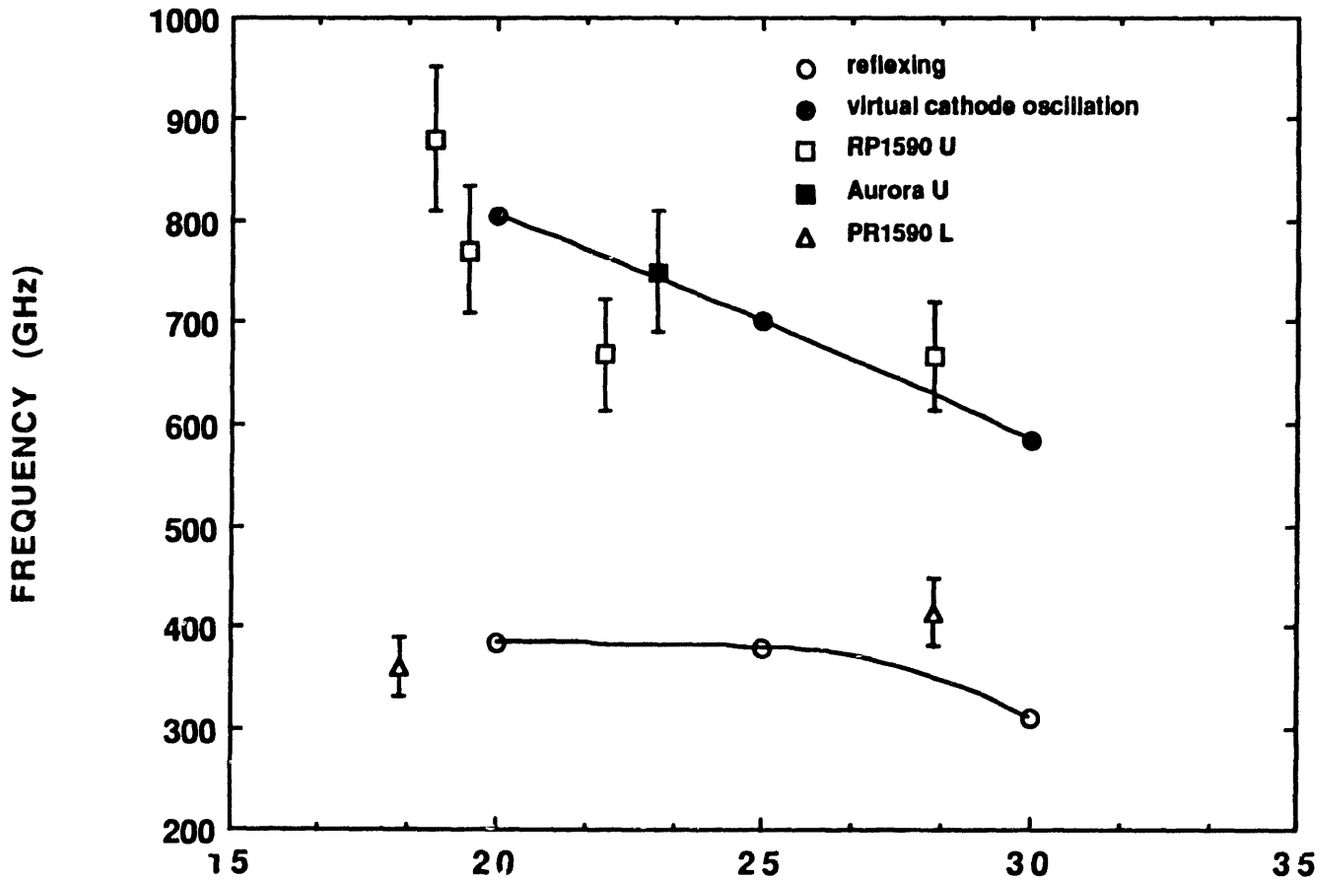

Fig. 6

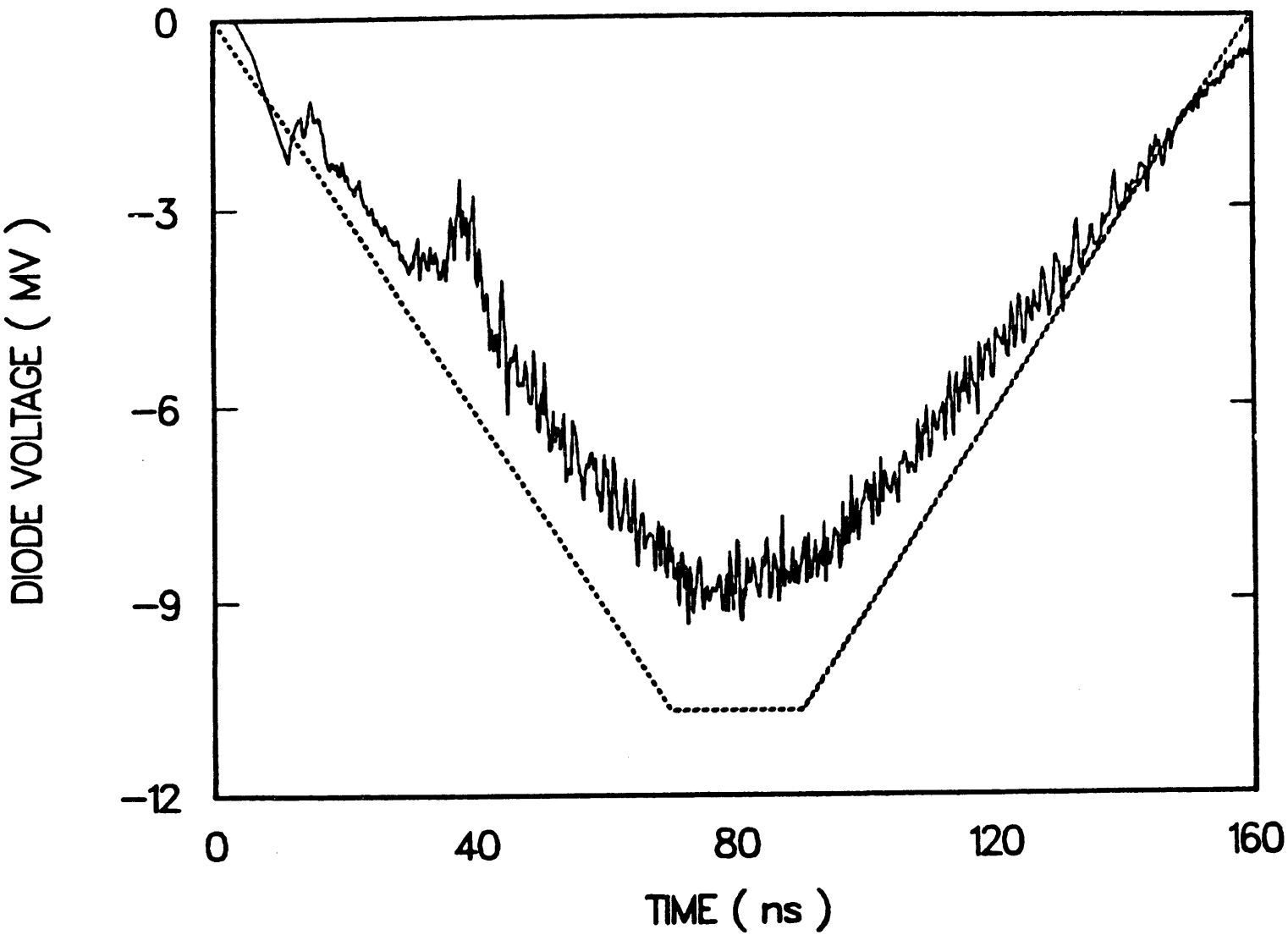

Fig. 4.

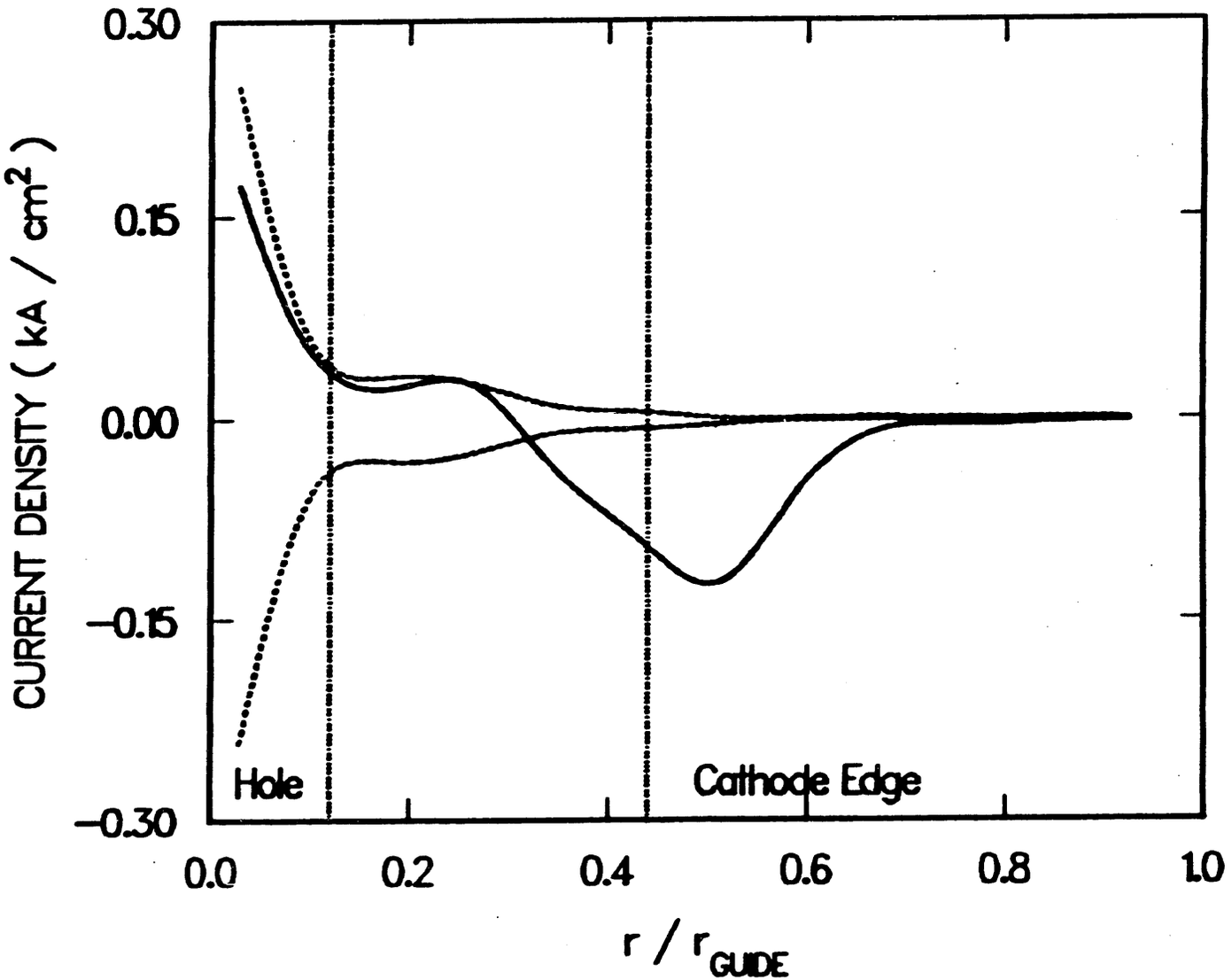
0.30
0.15
0.00
−0.15
−0.30
CURRENT DENSITY (kA / cm²)
Hole
Cathode Edge
0.0
0.2
0.4
0.6
0.8
1.0
r / r GUIDE

END

DATE
FILMED
11/08/91